Computer Assisted Mechanics and Engineering Sciences, **10**: 117–137, 2003.

Compliance optimization of the truss structures[†]

Sławomir Czarnecki
Institute of Structural Mechanics, Warsaw University of Technology
Al. Armii Ludowej 16, 00-637 Warsaw, Poland

(Received October 25, 2002)

The paper discusses the problem of designing the stiffest truss with a given and fixed number of joints and element connections. The design variables are the cross sectional areas of the bars or/and the nodal points locations. In each case a maximal volume of a truss, constituting an isoperimetric unilateral condition is prescribed. The nodal force vector is assumed to be independent of the design variables, hence fixed during the optimization process. The equilibrium problems of the trusses are modeled by the conventional linear as well as nonlinear finite element analyses taking into account large nodal displacements and small deformations of members. New optimal layouts of plane and space trusses are presented. These new layouts are found by using the moving asymptotes algorithm, the simplex method and the optimality criteria method.

1. Introduction

Topology optimization of trusses is a classical subject in structural design. In the past decade, the main effort of the researchers was focused on problems with a large number of potential structural elements, using the so-called ground structure approach in which the layout of a truss structure is found by allowing a certain set of connections between a fixed set of nodal points as potential structural or vanishing members [2]. This means that the positions of the nodal points are not used as design variables, so for the most part, the interesting and valuable solutions of efficient topologies can be obtained only in the case of a really large number of potential structural elements. This has to be done in order to simulate variable nodal positions while finding only the optimal cross sectional areas of the bars (with zero lower bounds imposed). Consequently, the simplest possible optimal design problem, namely the minimization of compliance (maximization of stiffness) for a given total volume of the structure is most often considered. At present, this problem can be given in a number of equivalent problem statements for which very efficient algorithms are derived that can handle truss structures with a large number of bars. A drawback of these methods is the assumption of a constant nodal layout and member connections during the optimization process. Indeed, many numerical tests confirm that the optimal topologies can be very sensitive to the fixed layout of nodal points especially if their number is relatively low [2]. Thus, as a consequence, it seems to be quite natural to consider an extension of the previous problem formulation by including additionally the optimization of the nodal point position, called the geometry optimization. Thus the process of finding the optimal topology and geometry of the structure becomes of course much more complicated – the geometrical design variables enter the problem in a nonlinear, non-convex – and in some formulations – in a non-smooth manner. But even in this case the tools have been developed capable of handling this problem with a relatively big number of elements. However, let us notice, that by combining topology and geometry optimization methods it is possible to avoid the growing up difficulties by choosing the initial ground structure much more sparse if the nodal positions are not fixed but also enter the optimization process as design variables. The question appears how far

[†]This is an extended version of a paper presented at the conference *OPTY-2001, Mathematical and Engineering Aspects of Optimal Design of Materials and Structures*, Poznań, Poland, August 27–29, 2001.

the number of elements can be safely reduced and give a still relatively good optimal solutions but in an easier way and at a lower computational cost? The full answer is unknown, but numerical experiments suggest that in many cases the significant reduction of the bars in the layout of the structures does not only facilitate the optimization process but also allows to obtain satisfactory solutions – competitive in comparison with the well known examples available in the literature. Another point is which algorithms and numerical tools should be applied. In the paper we devise new sensitivity formulae for geometrically linear and nonlinear trusses. Having these formulae at our disposal we can work out a new numerical procedure based on the method of moving asymptotes [15]. These sensitivities formulae can be applied in any gradient algorithm.

Let us consider a truss composed of M members and N nodes, subjected to the conservative nodal forces $\mathbf{Q} \in R^D$. The problem of finding the coordinates of nodes $\mathbf{X} \in R^D$ (geometry optimization) and the volumes $\mathbf{V} = \mathbf{V}(\mathbf{X}) \in R^M$ of the members (topology optimization) for which the nodal displacement vector $\mathbf{q} \in R^D$ minimizes the truss compliance $\mathbf{Q} \cdot \mathbf{q}$ under the condition of the truss volume being smaller than a fixed volume V is formulated as follows [1],

$$\min_{\mathbf{V}\in R^M,\, \mathbf{X}\in R^D,\, \mathbf{q}\in\Phi} \left\{ \mathbf{Q}\cdot\mathbf{q} \;\middle|\; \mathbf{K}(\mathbf{V},\mathbf{X})\mathbf{q} = \mathbf{Q},\;\; \mathbf{V} \geq \mathbf{0},\;\; \sum_{e=1}^{M} V_e \leq V,\;\; \mathbf{X} \in F \right\}. \tag{1}$$

Here $D = d \cdot N$ ($d = 2$ in the plane case and $d = 3$ in the spatial case) represents the number of the total degrees of freedom of a truss, $\mathbf{K} = \mathbf{K}(\mathbf{V},\mathbf{X}) \in \mathbf{M}_{D\times D}$ represents its stiffness matrix, $\Phi \subset R^D$ is a subspace of all vectors in R^D with a zero "boundary displacement" components and $F \subset R^D$ is a region of feasible position of nodes. The dot "$\cdot$" means the scalar product in R^D. The nodal displacement vector $\mathbf{q}$ is treated in Eq. (1) as an additional, independent variable of the optimization problem. Such approach makes it possible to solve effectively the following equivalent problem:

$$\min_{\mathbf{X}\in R^D} \{h(\mathbf{X}) \mid \mathbf{X} \in F\} \tag{2}$$

where the function $h(\cdot)$ defined on R^D reads

$$h(\mathbf{X}) = \min_{V\in R^M, \mathbf{q}\in\Phi} \left\{ \mathbf{Q}\cdot\mathbf{q} \;\middle|\; \mathbf{K}(\mathbf{V},\mathbf{X})\mathbf{q} = \mathbf{Q},\;\; \mathbf{V} \geq \mathbf{0},\;\; \sum_{e=1}^{M} V_e \leq V \right\}. \tag{3}$$

Due to the condition of volume members being non-negative the formulation above admits vanishing of some members. The stiffness matrix of such a truss is in general, semi positive definite. Finding the value of the function (3) above is equivalent to solving the topology optimization problem for $\mathbf{X}$ fixed. The applied algorithms should treat the nodal displacement vector $\mathbf{q}$ as an independent design variable – thus omitting the need of inverting the stiffness matrix $\mathbf{K}$, as it is characteristic e.g. for the simplex method, cf. [1]. Thus the values $h = h(\mathbf{X})$ determine the values of the objective function for the following design variables

$$\mathbf{V} = \mathbf{V}(\mathbf{X}), \mathbf{q} = \mathbf{q}(\mathbf{X}). \tag{4}$$

It is well known that the non-linear function $h(\cdot)$ is non-convex and non-smooth, cf. [1]. None the less the efficient iterative minimization algorithms can also be applied in this case but we can only expect to obtain local minima of (3).

On the other hand, for the trusses composed of all possible members linking all nodes from a given set and under the condition of a fixed vector $\mathbf{X}$, an optimal modeling involving the shape of the truss is still possible, because we can practically eliminate bars and change the initial topology of the structure – the way the nodes are linked by members. But the computational complexity problem is associated with the number of unknowns expressed by the formula $N(N-1)/2$, which represents a big number, indeed. For instance, for a truss of $N = 1000$ this number is of order 500 000.

Taking the above into account let us note that if the problem (1) is augmented by treating the nodal coordinates as unknowns, then the reduction of the number of truss members by considering the layouts in which only the neighbouring nodes are linked turns out to be a compromise approach giving convergent sequence of approximate solutions tending faster to the true optimal solutions. By taking the number of truss members smaller the optimal solutions become more sensitive to geometry changes. Then the number of design variables is essentially smaller thus justifying application of the conventional gradient methods of the nonlinear programming which work only for moderate problem size [1]. For instance, in the layout where only neighbouring nodes are interconnected and $N = 1000$ the number of design variables is of order 6000. Moreover, such approach is justified in the geometrically nonlinear cases when the known formulations of the topology optimization problems [1, 2] do not encompass the case considered. Due to the dyadic form of the stiffness matrix of a truss the formulae of the sensitivity analysis can be easy derived by using the known theorems of the advanced calculus.

The objectives of the paper are:

- derivation of the formulae for the gradients of truss compliance in the geometrically linear as well as nonlinear cases
- application of the derived sensitivity formulae in the moving asymptotes method [15], in the topology and shape optimization of selected plane and spatial trusses
- application of the simplex method and optimality criteria method [1, 2] in the topology optimization of selected plane and spatial trusses (only in geometrically linear case).

The presented results of the first goal of the paper seem to be new in the case of the $\mathbf{X}$ vector treated as unknown, especially in the geometrically non-linear case. Moreover, the computation of the gradients with respect to the vector of cross-sections $\mathbf{A} \in R^M$ as a design variable is very simple in the geometrically linear case, so only in the geometrically non-linear case the derived formulae can be viewed as fully original.

2. THE EQUILIBRIUM EQUATIONS OF TRUSSES IN THE LINEAR AND NONLINEAR RANGES

Assume the case of a spatial truss, i.e. $d = 3$. If referred to the global coordinate system the equilibrium equations can be easy formulated, if one introduces the following linear mapping

$$\mathbf{T}^e : R^D \to R^D, \qquad e = 1, \ldots, M, \tag{5}$$

defined by the allocation matrix $\mathbf{H} \in \mathbf{M}_{M\times 2}$ and the matrix $\mathbf{G} \in \mathbf{M}_{(2\cdot d)\times(2\cdot d)}$ defined below. The component $\mathbf{H}[e,k] \in \{1,\ldots,N\}$, $e = 1,\ldots,M$, represents the number of a node (referred to the global numeration) which in the e-th member has locally a smaller number for $k = 1$ or higher for $k = 2$. The matrix $\mathbf{G}$ is symmetric [3] and is given by

$$\mathbf{G} = \begin{bmatrix} 1 & 0 & 0 & -1 & 0 & 0 \\ 0 & 1 & 0 & 0 & -1 & 0 \\ 0 & 0 & 1 & 0 & 0 & -1 \\ -1 & 0 & 0 & 1 & 0 & 0 \\ 0 & -1 & 0 & 0 & 1 & 0 \\ 0 & 0 & -1 & 0 & 0 & 1 \end{bmatrix}. \tag{6}$$

Let us define the matrices $\mathbf{U}^n \in \mathbf{M}_{d\times D}$, $n \in \{1,\ldots,N\}$ and $\mathbf{G}^e \in \mathbf{M}_{(2\cdot d)\times D}$, $e \in \{1,\ldots,M\}$:

$$\mathbf{U}^{\mathbf{H}[e,k]}[i,j] = \begin{cases} 1 & \text{if } [i,j] = [1, 3\cdot\mathbf{H}[e,k]-2] \text{ or } [2, 3\cdot\mathbf{H}[e,k]-1] \text{ or } [3, 3\cdot\mathbf{H}[e,k]-0], \\ 0 & \text{in other cases} \end{cases} \tag{7}$$
$$(i = 1,\ldots,d,\ j = 1,\ldots,D),$$

$$\mathbf{G} = \begin{bmatrix} \mathbf{U}^{\mathbf{H}[e,1]} \\ \mathbf{U}^{\mathbf{H}[e,2]} \end{bmatrix}. \tag{8}$$

Matrices $\mathbf{T}^e$ are defined as follows

$$\mathbf{T}^e = (\mathbf{G}^e)^T \mathbf{G}\mathbf{G}^e, \qquad e \in \{1,\ldots,M\}, \tag{9}$$

where $(\cdot)^T$ means transposition, while the length of the e-th bar can be then expressed by

$$L_e(\mathbf{X}) = \sqrt{\mathbf{T}^e\mathbf{X}\cdot\mathbf{X}}, \qquad e = 1,\ldots,M. \tag{10}$$

Introduction of the matrices $\mathbf{T}^e$ allows us to express, for the each e-th bar, the results of the respective differences between the local Cartesian coordinates of the nodes in D dimensional (global) vectors. The matrices $\mathbf{T}^e$ considerably simplify the notion of the assembly process required to construct global stiffness matrix and load vector. Moreover, the left hand side of the equilibrium equation (see Eqs. (12)–(15) below) can be easily written and interpreted as a result of action of an operator

$$\mathbf{B} : R^{M+D} \to R^D \tag{11}$$

from the space R^{M+D} of the design variables $(\mathbf{A},\mathbf{X}) \in R^M \times R^D$ into the space R^D. Such a global representation of the equilibrium equation makes the interpretation of the sensitivity analysis results clear and justifiable.

The elastic equilibrium equation for the geometrically linear case has the form

$$\mathbf{K}(\mathbf{A},\mathbf{X})\,\mathbf{q}(\mathbf{A},\mathbf{X}) = \mathbf{Q} \tag{12}$$

where the stiffness matrix $\mathbf{K}(\mathbf{A},\mathbf{X}) \in \mathbf{M}_{D\times D}$ is symmetric and is given by

$$\mathbf{K}(\mathbf{A},\mathbf{X}) = \sum_{e=1}^{M} \frac{E\cdot A_e}{L_e(\mathbf{X})^3}\,\mathbf{T}^e(\mathbf{X}) \otimes \mathbf{T}^e(\mathbf{X}). \tag{13}$$

Here $\mathbf{a}\otimes\mathbf{b}$ denotes the tensor product of the two vectors $\mathbf{a}$ and $\mathbf{b}$, or $(\mathbf{a}\otimes\mathbf{b})_{ij} = a_i b_j$.

The elastic equilibrium equation for the geometrically non-linear case in the total Lagrange formulation and for the truss element based on Green's strain has the form [3]

$$\mathbf{K}[\mathbf{A},\mathbf{X},\mathbf{q}(\mathbf{A},\mathbf{X})]\,\mathbf{q}(\mathbf{A},\mathbf{X}) = \mathbf{Q} \tag{14}$$

where, now not symmetric, the stiffness matrix has the form

$$\mathbf{K}[\mathbf{A},\mathbf{X},\mathbf{q}(\mathbf{A},\mathbf{X})] = \sum_{e=1}^{M} \frac{E\cdot A_e}{L_e(\mathbf{X})^3}\,\mathbf{T}^e\mathbf{X}\otimes\mathbf{T}^e\mathbf{X} + \frac{1}{2}\sum_{e=1}^{M} \frac{E\cdot A_e}{L_e(\mathbf{X})^3}\,\mathbf{T}^e\mathbf{X}\otimes\mathbf{T}^e\mathbf{q}$$
$$+ \sum_{e=1}^{M} \frac{E\cdot A_e}{L_e(\mathbf{X})^3}\,\mathbf{T}^e\mathbf{q}\otimes\mathbf{T}^e\mathbf{X} + \frac{1}{2}\sum_{e=1}^{M} \frac{E\cdot A_e}{L_e(\mathbf{X})^3}\,\mathbf{T}^e\mathbf{q}\otimes\mathbf{T}^e\mathbf{q}. \tag{15}$$

The tangent stiffness matrix turns out to be symmetric; it reads

$$\mathbf{K}_q[\mathbf{A},\mathbf{X},\mathbf{q}(\mathbf{A},\mathbf{X})] = \sum_{e=1}^{M} \frac{E\cdot A_e}{L_e(\mathbf{X})^3}\,\mathbf{T}^e\mathbf{X}\otimes\mathbf{T}^e\mathbf{X} + \sum_{e=1}^{M} \frac{E\cdot A_e}{L_e(\mathbf{X})^3}\,\mathbf{T}^e\mathbf{X}\otimes\mathbf{T}^e\mathbf{q}$$
$$+ \sum_{e=1}^{M} \frac{E\cdot A_e}{L_e(\mathbf{X})^3}\,\mathbf{T}^e\mathbf{q}\otimes\mathbf{T}^e\mathbf{X} + \sum_{e=1}^{M} \frac{E\cdot A_e}{L_e(\mathbf{X})^3}\,\mathbf{T}^e\mathbf{q}\otimes\mathbf{T}^e\mathbf{q}$$
$$+ \sum_{e=1}^{M} \frac{E\cdot A_e}{L_e(\mathbf{X})^3}\left(\mathbf{T}^e\mathbf{X}\cdot\mathbf{q} + \frac{1}{2}\mathbf{T}^e\mathbf{q}\cdot\mathbf{q}\right)\mathbf{T}^e. \tag{16}$$

Matrix (16) was computed by differentiation of the equilibrium equation (14) written as

$$\mathbf{C}(\mathbf{q}) = \mathbf{0} \tag{17}$$

with respect to the vector $\mathbf{q}\in R^D$. Here

$$\mathbf{C}: R^D \to R^D, \qquad \mathbf{C}(\mathbf{q}) = \mathbf{K}(\mathbf{q})\mathbf{q} - \mathbf{Q}, \tag{18}$$

where for the arbitrary but constant vector $(\mathbf{A},\mathbf{X})\in R^{M+D}$ the following notion is adopted

$$\mathbf{K}(\mathbf{q})\mathbf{q} = \mathbf{K}[\mathbf{A},\mathbf{X},\mathbf{q}(\mathbf{A},\mathbf{X})]\,\mathbf{q}(\mathbf{A},\mathbf{X}). \tag{19}$$

Indeed, by differentiating Eq. (17) with respect to the variable $\mathbf{q}$, it is not difficult to show that

$$\frac{\partial\mathbf{C}}{\partial\mathbf{q}}(\mathbf{q}) = \left[\frac{\partial\mathbf{K}}{\partial q_1}(\mathbf{q})\,\mathbf{q},\ \frac{\partial\mathbf{K}}{\partial q_2}(\mathbf{q})\,\mathbf{q},\ \ldots,\ \frac{\partial\mathbf{K}}{\partial q_D}(\mathbf{q})\,\mathbf{q}\right] + \mathbf{K}(\mathbf{q}) = \mathbf{K}_q[\mathbf{A},\mathbf{X},\mathbf{q}(\mathbf{A},\mathbf{X})]. \tag{20}$$

The matrix (16) as well as the two higher derivatives (with respect to $\mathbf{q}$) – second and third – can be used not only in the static analysis by applying e.g. Newton method in solving a nonlinear equation (14) but also in a stability analysis via Riks method [4, 14]. The boundary conditions in Eqs. (12), (14) (and matrices (13), (15), (16)) should be properly introduced according to the standard procedures of the FEM.

3. Sensitivity analysis

The derivation of the sensitivity formulae, based on the direct method, for the geometrically linear truss was presented in [5]. In the present paper, the counterparts of these results are considered for the geometrically non-linear structures and for the completeness of the presentation – also for geometrically linear case.

The partial derivatives $\frac{\partial}{\partial\mathbf{A}}(\cdots)$, $\frac{\partial}{\partial\mathbf{X}}(\cdots)$ of the objective function

$$f: R^M\times R^D\to R \qquad f(\mathbf{A},\mathbf{X}) = \mathbf{Q}\cdot\mathbf{q}(\mathbf{A},\mathbf{X}) \tag{21}$$

assume the form

$$\partial_{\mathbf{A}} f(\mathbf{A},\mathbf{X}) = [\partial_{\mathbf{A}}\mathbf{q}(\mathbf{A},\mathbf{X})]^T\mathbf{Q}, \tag{22}$$
$$\partial_{\mathbf{X}} f(\mathbf{A},\mathbf{X}) = [\partial_{\mathbf{X}}\mathbf{q}(\mathbf{A},\mathbf{X})]^T\mathbf{Q}. \tag{23}$$

Here the abbreviations $\partial_{\mathbf{A}}(\cdots) = \dfrac{\partial(\cdots)}{\partial \mathbf{A}}$, $\partial_{\mathbf{X}}(\cdots) = \dfrac{\partial(\cdots)}{\partial \mathbf{X}}$, are used. Upon appropriate introduction of the boundary conditions the matrices

$$\partial_{\mathbf{A}}\mathbf{q}(\mathbf{A},\mathbf{X}) = \begin{bmatrix} \dfrac{\partial q_1}{\partial A_1}(\mathbf{A},\mathbf{X}) & \cdots & \dfrac{\partial q_1}{\partial A_M}(\mathbf{A},\mathbf{X}) \\ \vdots & \ddots & \vdots \\ \dfrac{\partial q_D}{\partial A_1}(\mathbf{A},\mathbf{X}) & \cdots & \dfrac{\partial q_D}{\partial A_M}(\mathbf{A},\mathbf{X}) \end{bmatrix} \in \mathbf{M}_{D\times M}\,, \tag{24}$$

$$\partial_{\mathbf{X}}\mathbf{q}(\mathbf{A},\mathbf{X}) = \begin{bmatrix} \dfrac{\partial q_1}{\partial X_1}(\mathbf{A},\mathbf{X}) & \cdots & \dfrac{\partial q_1}{\partial X_D}(\mathbf{A},\mathbf{X}) \\ \vdots & \ddots & \vdots \\ \dfrac{\partial q_D}{\partial X_1}(\mathbf{A},\mathbf{X}) & \cdots & \dfrac{\partial q_D}{\partial X_D}(\mathbf{A},\mathbf{X}) \end{bmatrix} \in \mathbf{M}_{D\times D}\,, \tag{25}$$

become the partial derivatives of the vector function

$$\mathbf{q} : R^M \times R^D \to R^D \tag{26}$$

with respect to $\mathbf{A}$ and $\mathbf{X}$, respectively, see [5].

In the geometrically linear case we get

$$\partial_{\mathbf{A}}\mathbf{q}(\mathbf{A},\mathbf{X}) = -\mathbf{K}(\mathbf{A},\mathbf{X})^{-1}\,\mathbf{K}'_{\mathbf{A}}(\mathbf{A},\mathbf{X}), \tag{27}$$

$$\partial_{\mathbf{X}}\mathbf{q}(\mathbf{A},\mathbf{X}) = -\mathbf{K}(\mathbf{A},\mathbf{X})^{-1}\,\mathbf{K}'_{\mathbf{X}}(\mathbf{A},\mathbf{X}), \tag{28}$$

while in the geometrically non-linear case we obtain

$$\partial_{\mathbf{A}}\mathbf{q}(\mathbf{A},\mathbf{X}) = -\mathbf{K}_{\mathbf{q}}[\mathbf{A},\mathbf{X},\mathbf{q}(\mathbf{A},\mathbf{X})]^{-1}\,\mathbf{K}'_{\mathbf{A}}(\mathbf{A},\mathbf{X}), \tag{29}$$

$$\partial_{\mathbf{X}}\mathbf{q}(\mathbf{A},\mathbf{X}) = -\mathbf{K}_{\mathbf{q}}[\mathbf{A},\mathbf{X},\mathbf{q}(\mathbf{A},\mathbf{X})]^{-1}\,\mathbf{K}'_{\mathbf{X}}(\mathbf{A},\mathbf{X}). \tag{30}$$

For the geometrically linear case we have

$$\mathbf{K}'_{\mathbf{A}}(\mathbf{A},\mathbf{X}) = \sum_{e=1}^{M} \frac{E}{L_e(\mathbf{X})^3}(\mathbf{T}^e\mathbf{X}\cdot\mathbf{q})\mathbf{T}^e\mathbf{X}\otimes\mathbf{i}_e\,, \tag{31}$$

$$\begin{aligned}\mathbf{K}'_{\mathbf{X}}(\mathbf{A},\mathbf{X}) = &\sum_{e=1}^{M} -\frac{3\cdot E\cdot A_e}{L_e(\mathbf{X})^5}(\mathbf{T}^e\mathbf{X}\cdot\mathbf{q})\mathbf{T}^e\mathbf{X}\otimes\mathbf{T}^e\mathbf{X} \\ &+\sum_{e=1}^{M}\frac{E\cdot A_e}{L_e(\mathbf{X})^3}(\mathbf{T}^e\mathbf{X}\cdot\mathbf{q})\mathbf{T}^e + \sum_{e=1}^{M}\frac{E\cdot A_e}{L_e(\mathbf{X})^3}\mathbf{T}^e\mathbf{X}\otimes\mathbf{T}^e\mathbf{q}\end{aligned} \tag{32}$$

while in the geometrically non-linear case one gets

$$\begin{aligned}\mathbf{K}'_{\mathbf{A}}(\mathbf{A},\mathbf{X}) = &\sum_{e=1}^{M}\frac{E}{L_e(\mathbf{X})^3}\left(\mathbf{T}^e\mathbf{X}\cdot\mathbf{q}+\frac{1}{2}\mathbf{T}^e\mathbf{q}\cdot\mathbf{q}\right)\mathbf{T}^e\mathbf{X}\otimes\mathbf{i}_e \\ &+\sum_{e=1}^{M}\frac{E}{L_e(\mathbf{X})^3}\left(\mathbf{T}^e\mathbf{X}\cdot\mathbf{q}+\frac{1}{2}\mathbf{T}^e\mathbf{q}\cdot\mathbf{q}\right)\mathbf{T}^e\mathbf{q}\otimes\mathbf{i}_e\,,\end{aligned} \tag{33}$$

$$\mathbf{K}'_{\mathbf{X}}(\mathbf{A},\mathbf{X}) = \sum_{e=1}^{M} \frac{-3E\cdot A_e}{L_e(\mathbf{X})^5}\left(\mathbf{T}^e\mathbf{X}\cdot\mathbf{q}+\frac{1}{2}\mathbf{T}^e\mathbf{q}\cdot\mathbf{q}\right)\mathbf{T}^e\mathbf{X}\otimes\mathbf{T}^e\mathbf{X}+\sum_{e=1}^{M}\frac{E\cdot A_e}{L_e(\mathbf{X})^3}\mathbf{T}^e\mathbf{X}\otimes\mathbf{T}^e\mathbf{q}$$
$$+\sum_{e=1}^{M}\frac{-3E\cdot A_e}{L_e(\mathbf{X})^5}\left(\mathbf{T}^e\mathbf{X}\cdot\mathbf{q}+\frac{1}{2}\mathbf{T}^e\mathbf{q}\cdot\mathbf{q}\right)\mathbf{T}^e\mathbf{q}\otimes\mathbf{T}^e\mathbf{X}+\sum_{e=1}^{M}\frac{E\cdot A_e}{L_e(\mathbf{X})^3}\mathbf{T}^e\mathbf{q}\otimes\mathbf{T}^e\mathbf{q}$$
$$+\sum_{e=1}^{M}\frac{E\cdot A_e}{L_e(\mathbf{X})^3}\left(\mathbf{T}^e\mathbf{X}\cdot\mathbf{q}+\frac{1}{2}\mathbf{T}^e\mathbf{q}\cdot\mathbf{q}\right)\mathbf{T}^e, \tag{34}$$

with $\mathbf{i}_e$ being a vector of the unit orthogonal basis in R^M.

Moreover, the derivatives of the volume of the structure

$$\Omega : R^M\times R^D\to R, \Omega(\mathbf{A},\mathbf{X}) = \mathbf{A}\cdot\mathbf{L}(\mathbf{X}) \tag{35}$$

assume the forms

$$\partial_{\mathbf{A}}\Omega(\mathbf{A},\mathbf{X}) = \mathbf{L}(\mathbf{X}), \tag{36}$$

$$\partial_{\mathbf{X}}\Omega(\mathbf{A},\mathbf{X}) = \sum_{e=1}^{M}\frac{A_e}{L_e(\mathbf{X})}\mathbf{T}^e\mathbf{X}. \tag{37}$$

The partial derivatives of the bar stresses ($e=1,\ldots,M$)

$$\sigma_e(\mathbf{A},\mathbf{X}) = \frac{E}{L_e(\mathbf{X})^2}\mathbf{T}^e\mathbf{X}\cdot\mathbf{q} \tag{38}$$

in the geometrically linear case and

$$\sigma_e(\mathbf{A},\mathbf{X}) = \frac{E}{[L_e(\mathbf{X})]^2}\left(\mathbf{T}^e\mathbf{X}\cdot\mathbf{q}+\frac{1}{2}\mathbf{T}^e\mathbf{q}\cdot\mathbf{q}\right) \tag{39}$$

in the geometrically non-linear case assume the form

$$\partial_{\mathbf{A}}\sigma_e(\mathbf{A},\mathbf{X}) = \frac{E}{[L_e(\mathbf{X})]^2}[\partial_{\mathbf{A}}\mathbf{q}(\mathbf{A},\mathbf{X})]^T\mathbf{T}^e\mathbf{X}, \tag{40}$$

$$\partial_{\mathbf{X}}\sigma_e(\mathbf{A},\mathbf{X}) = -\frac{2E}{[L_e(\mathbf{X})]^4}(\mathbf{T}^e\mathbf{X}\cdot\mathbf{q})\mathbf{T}^e\mathbf{X}+\frac{E}{[L_e(\mathbf{X})]^2}\mathbf{T}^e\mathbf{q}+\frac{E}{[L_e(\mathbf{X})]^2}[\partial_{\mathbf{X}}\mathbf{q}(\mathbf{A},\mathbf{X})]^T\mathbf{T}^e\mathbf{X}, \tag{41}$$

in the geometrically linear case and the following form,

$$\partial_{\mathbf{A}}\sigma_e(\mathbf{A},\mathbf{X}) = \frac{E}{[L_e(\mathbf{X})]^2}[\partial_{\mathbf{A}}\mathbf{q}(\mathbf{A},\mathbf{X})]^T(\mathbf{T}^e\mathbf{X}+\mathbf{T}^e\mathbf{q}), \tag{42}$$

$$\partial_{\mathbf{X}}\sigma_e(\mathbf{A},\mathbf{X}) = -\frac{2E}{[L_e(\mathbf{X})]^4}\left(\mathbf{T}^e\mathbf{X}\cdot\mathbf{q}+\frac{1}{2}\mathbf{T}^e\mathbf{q}\cdot\mathbf{q}\right)\mathbf{T}^e\mathbf{X}$$
$$+\frac{E}{[L_e(\mathbf{X})]^2}\mathbf{T}^e\mathbf{q}+\frac{E}{[L_e(\mathbf{X})]^2}[\partial_{\mathbf{X}}\mathbf{q}(\mathbf{A},\mathbf{X})]^T(\mathbf{T}^e\mathbf{X}+\mathbf{T}^e\mathbf{q}), \tag{43}$$

in the geometrically non-linear case, respectively.

The partial derivatives of the member forces

$$F_e(\mathbf{A},\mathbf{X}) = A_e\sigma_e(\mathbf{A},\mathbf{X}),\qquad e=1,\ldots,M, \tag{44}$$

assume the form

$$\partial_{\mathbf{A}}F_e(\mathbf{A},\mathbf{X}) = \sigma_e(\mathbf{A},\mathbf{X})\mathbf{i}_e + A_e\,\partial_{\mathbf{A}}\sigma_e(\mathbf{A},\mathbf{X}), \tag{45}$$

$$\partial_{\mathbf{X}}F_e(\mathbf{A},\mathbf{X}) = A_e\,\partial_{\mathbf{X}}\sigma_e(\mathbf{A},\mathbf{X}). \tag{46}$$

The correctness of the sensitivity formulae (27)–(30), (40)–(43), (45), (46) were additionally numerically checked by using the mathematical definition of the gradient, e.g. the k-th column of the matrix (25) (i.e. (28) or (30)) is equal to

$$\begin{bmatrix} \dfrac{\partial q_1}{\partial X_k}(\mathbf{A},\mathbf{X}) \\ \vdots \\ \dfrac{\partial q_D}{\partial X_k}(\mathbf{A},\mathbf{X}) \end{bmatrix} = \partial_{\mathbf{X}}\mathbf{q}(\mathbf{A},\mathbf{X})[\mathbf{i}_k] \cong \frac{\mathbf{q}(\mathbf{A},\mathbf{X}+t\mathbf{i}_k)-\mathbf{q}(\mathbf{A},\mathbf{X})}{t} \tag{47}$$

for "sufficiently" small parameter t, with $\mathbf{i}_k$ $(k=1,\ldots,D)$ being a vector of the unit orthogonal basis in R^D. Moreover, the relation (47) hints at the appropriate dependence on the boundary conditions in matrix (25) – the rows with indices labeling the fixed nodal coordinates must be set to zero. In the geometrically non-linear case, the derived sensitivity formulae should be used with a great care, because the solution of the (non-linear) equilibrium equation (14) is in general not unique for a given load vector $\mathbf{Q}$.

4. Optimization methods

In the paper the three optimization methods are applied:

- Method of moving asymptotes (MMA) [15]
- Simplex method (SX) [1, 2]
- Optimality criteria method (OC) [2]

4.1. Method of moving asymptotes

The design variables are: the vector of cross sections $\mathbf{A} \in R^M$ or/and the coordinates of nodes $\mathbf{X} \in R^D$. In general the vector $(\mathbf{A},\mathbf{X}) \in R^{M+D}$ represents the design variables. Using of the sensitivity formulae in the MMA necessitates the knowledge of all components of the displacement vector $\mathbf{q}$. Thus we treat this vector as a function of $(\mathbf{A},\mathbf{X})$ and the problem P of minimum compliance, in the geometrically linear case, assumes the following form,

$$\min_{\mathbf{A}\in R^M,\,\mathbf{X}\in R^D}\{\mathbf{Q}\cdot\mathbf{q}(\mathbf{A},\mathbf{X}) \mid \mathbf{K}(\mathbf{A},\mathbf{X})\,\mathbf{q}(\mathbf{A},\mathbf{X})=\mathbf{Q},\ \ \mathbf{A}\geq\mathbf{A}_{\min},\ \ \mathbf{A}\cdot\mathbf{L}(\mathbf{X})\leq V,\ \ \mathbf{X}\in F\}, \tag{48}$$

where $\mathbf{L}=\mathbf{L}(\mathbf{X})\in R^M$ represents a vector of member lengths and $\mathbf{A}_{\min}\in R^M$ stands for the vector of minimal cross sections. Its components are assumed to be positive, which is symbolically written as $\mathbf{A}_{\min}>\mathbf{0}$. Additionally, the set F of admissible coordinates of the nodes is taken such that the matrix $\mathbf{K}$ be positive definite at each step of the algorithm, so the displacement vector

$$\mathbf{q}(\mathbf{A},\mathbf{X})=\mathbf{K}^{-1}(\mathbf{A},\mathbf{X})\mathbf{Q} \tag{49}$$

can be found in each iteration loop.

In the geometrically non-linear case, we formulate the problem P similarly,

$$\min_{\mathbf{A}\in R^M,\mathbf{X}\in R^D}\{\mathbf{Q}\cdot\mathbf{q}(\mathbf{A},\mathbf{X}) \mid \mathbf{K}[\mathbf{A},\mathbf{X},\mathbf{q}(\mathbf{A},\mathbf{X})]\,\mathbf{q}(\mathbf{A},\mathbf{X})=\mathbf{Q},\quad \mathbf{A}\geq\mathbf{A}_{\min},\ \ \mathbf{A}\cdot\mathbf{L}(\mathbf{X})\leq V,\ \ \mathbf{X}\in F\}, \tag{50}$$

being aware of the rising computational difficulties.

In our problem P, the following iterative scheme generates and solves a sequence of explicit subproblems:

Step 0. Choose a starting, feasible point $(\mathbf{A}^0, \mathbf{X}^0)$ and put the iteration index $k = 0$.

Step 1. Given an iteration point $(\mathbf{A}^k, \mathbf{X}^k)$, calculate $f(\mathbf{A}^k, \mathbf{X}^k)$, $\Omega(\mathbf{A}^k, \mathbf{X}^k)$ according to Eqs. (21), (35) and the gradients $\nabla f(\mathbf{A}^k, \mathbf{X}^k)$, $\nabla\Omega(\mathbf{A}^k, \mathbf{X}^k)$ solving the equilibrium equation (12) or (14) together with the use of the sensitivity formulae (22), (23), (27), (28), (36), (37).

Step 2. Generate a subproblem P^k by replacing, in P, the functions $f(\cdot)$, $\Omega(\cdot)$ by approximating function $f^k(\cdot)$, $\Omega^k(\cdot)$, based on the calculations from step 1.

Step 3. Find the solution $(\mathbf{A}_k, \mathbf{X}_k)$ of the subproblem P^k. Substitute $(\mathbf{A}^{k+1}, \mathbf{X}^{k+1}) = (\mathbf{A}_k, \mathbf{X}_k)$, $k = k + 1$, and go to step 1.

The process is usually interrupted when some convergence criteria are fulfilled. The MMA defines functions $f^k(\cdot)$, $\Omega^k(\cdot)$ and gives answer to the question: how the subproblem P^k should be solved. In the past decade, many new versions of the original MMA were proposed. In the paper only the original form of MMA [15] has been used.

4.2. Simplex method

The design variable are the volumes $\mathbf{V} \in R^M$ of the members. In this case, we treat vector $\mathbf{q}$ as an additional independent variable and the problem P of minimum compliance assumes the following form,

$$\min_{\mathbf{V}\in R^M,\, \mathbf{q}\in\Phi} \left\{ \frac{1}{2}\mathbf{Q}\cdot\mathbf{q} \;\middle|\; \mathbf{K}(\mathbf{V})\mathbf{q} = \mathbf{Q},\;\; \mathbf{V} \geq \mathbf{0},\;\; \sum_{e=1}^{M} V_e \leq V \right\}, \tag{51}$$

where

$$\mathbf{K}(\mathbf{V}) = \sum_{e=1}^{M} V_e \frac{E}{L_e(\mathbf{X})^2}\, \mathbf{B}_e(\mathbf{X}) \otimes \mathbf{B}_e(\mathbf{X}) \tag{52}$$

is the stiffness matrix (13) and

$$\mathbf{B}(\mathbf{X}) = [\mathbf{B}_1(\mathbf{X}), \ldots, \mathbf{B}_M(\mathbf{X})] = \left[\frac{\mathbf{T}^1(\mathbf{X})}{L_1(\mathbf{X})}, \ldots, \frac{\mathbf{T}^M(\mathbf{X})}{L_M(\mathbf{X})} \right] \in \mathbf{M}_{D\times M} \tag{53}$$

represents a compatibility matrix with columns $\mathbf{B}_e(\mathbf{X})$, $e = 1, \ldots, M$.

According to [1, 2] the linear programming (LP) problem (weight minimization)

$$\min_{\mathbf{V}\in R^M,\, \mathbf{N}\in R^M} \left\{ \sum_{e=1}^{M} V_e \;\middle|\; \mathbf{BN} = \mathbf{Q},\;\; \mathbf{V} \geq \mathbf{0},\;\; \forall e \in \{1, \ldots, M\}\;\; |L_e N_e| \leq \sigma^{\max} V_e \right\} \tag{54}$$

and dual to (54) the linear programming problem

$$\max_{\mathbf{q}\in\Phi} \left\{ \mathbf{Q}\cdot\mathbf{q} \;\middle|\; \forall e \in \{1, \ldots, M\} \;\; \left| \frac{\mathbf{B}_e \cdot \mathbf{q}}{L_e} \right| \leq \frac{L_e}{\sigma^{\max}} \right\} \tag{55}$$

are equivalent to the original problem (51). The equivalence between problems (51) and (54) is not self-evident [1, 2]. In the above formulations, $\mathbf{N} \in R^M$ represents the member force vector and $\sigma^{\max} > 0$ denotes allowable stress for tension and compression. Due to the fact that (54) and (55) are linear programming problems, one can easily apply e.g. simplex method to find the solutions. Putting formally $\sigma^{\max} = \sqrt{E}$ and denoting the solutions of the above LP problems (54), (55) by

$(\mathbf{V}^*, \mathbf{N}^*) \in R^M \times R^M$ and $\mathbf{q}^* \in \Phi$ respectively, the solution $(\mathbf{V}, \mathbf{q}) \in R^M \times \Phi$ of the original problem (51) has the following form,

$$(\mathbf{V}, \mathbf{q}) = \left(\frac{V}{\sum_{e=1}^{M} V_e^*} \mathbf{V}^*, \frac{\sum_{e=1}^{M} V_e^*}{V} \mathbf{q}^* \right). \tag{56}$$

In particular, the best minimal compliance is equal to $\mathbf{Q} \cdot \mathbf{q}$ and the optimal cross sectional areas of the bars are $A_e = V_e / L^e$, $(e = 1, \ldots, M)$.

4.3. Optimality criteria method

The design variables are the volumes of the members forming the vector $\mathbf{V} \in R^M$. The problem P of minimum compliance assumes the following form,

$$\min_{\mathbf{V} \in R^M} \left\{ \mathbf{Q} \cdot \mathbf{q}(\mathbf{V}) \;\middle|\; \mathbf{K}(\mathbf{V})\, \mathbf{q}(\mathbf{V}) = \mathbf{Q}, \quad \mathbf{V} \geq \mathbf{V}_{\min}, \quad \sum_{e=1}^{M} V_e = V \right\}, \tag{57}$$

where $\mathbf{V}_{\min} \in R^M$ stands for the vector of minimal member volumes. Its components are assumed to be positive, which is symbolically written as $\mathbf{V}_{\min} > \mathbf{0}$ (which assures positive definiteness of the stiffness matrix $\mathbf{K}$). For this formulation an effective algorithm called optimality criteria method is very often used. The method assigns material (volumes) to members proportionally to the specific energy of each member in order to reach the situation of constant specific energy in the active bars [2]. Another interpretation of the method can be viewed as a fully stressed design because in each e-th bar contained in the optimal structure, its stress is maximal among all bars in the structure (corollary from the Theorem 2.5 in [1]). The k-th iteration step consists of the following commands [2]:

1. for given $\mathbf{V}^{k-1} = (V_e^{k-1})_{e=1,2,\ldots,M}$ compute displacement $\mathbf{q}^{k-1}$ from the equilibrium equation (12),

2. find Lagrange multiplier Λ such that

$$\sum_{e=1}^{M} \max \left\{ V_e^{k-1} \frac{E}{L_e^2} \frac{\mathbf{B}_e \mathbf{q}^{k-1} \cdot \mathbf{B}_e \mathbf{q}^{k-1}}{\Lambda}, V_{\min} \right\} = V, \tag{58}$$

3. update

$$\forall e \in \{1, 2, \ldots, M\} \quad V_e^k = \max \left\{ V_e^{k-1} \frac{E}{L_e^2} \frac{\mathbf{B}_e \mathbf{q}^{k-1} \cdot \mathbf{B}_e \mathbf{q}^{k-1}}{\Lambda}, V_{\min} \right\}. \tag{59}$$

5. Case studies

The described methods are demonstrated for the plane and space truss structures. In some cases of the topology optimization, the results of the two or three algorithms (MMA, SX, OC) are compared. In all of the presented examples the ground structures admit the connections to the neighbouring nodes (see Fig. 1) but the case of all possible connections between all nodes is also presented. Most of the presented solutions was obtained on the basis of the MMA and this algorithm was mainly tested.

In Fig. 1 the two examples of the initial layout of the bars are shown, applied in the truss optimization from Figs. 2–18. These layouts define Cartesian patterns, to be projected by means of the appropriate mapping onto required type of a shell. In the case of rotational symmetrical grid

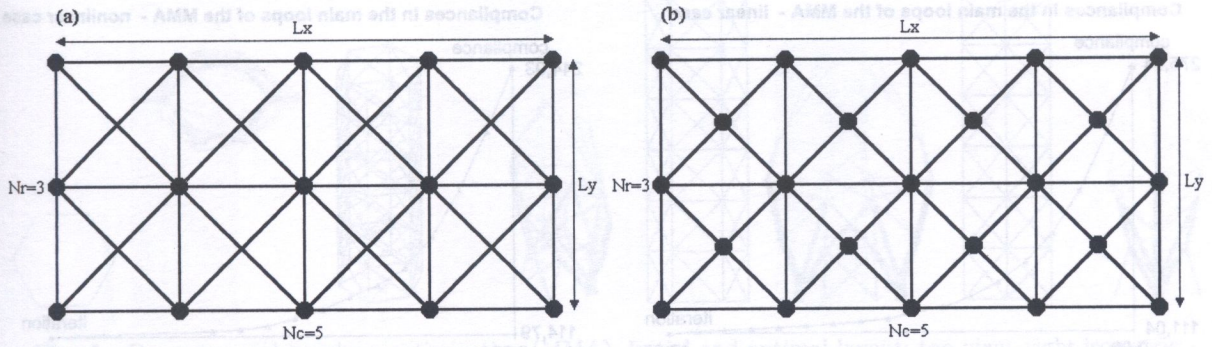

Fig. 1. Two types of the initial patterns with 15 and 23 nodes in (a) and (b) respectively

shells, the first and last columns of nodes in Fig. 1 (shell meridians) are identified and the number of rows "defines" the height of the shell (N_r, N_c, L_x, L_y, represent the number of rows, columns of the nodes, the length of the grid in x and y directions respectively).

The program including statics of the geometrically linear and non-linear trusses was written in C++. Optimization procedures were written in Java. One dimensional optimization procedures and simplex method were adopted from [13]. Graphical procedures were written in Java language and in Basic language compiled in MicroStation95 programming environment.

The thicknesses of the bars are scaled in such a way that the thicker and darker line refers to the greater cross-section. The initial cross sectional areas of the bars are equal to $4.0 \cdot 10^{-6}$ [m^2]. The components of the vector $\mathbf{A}_{\min} \in R^M$ in Eqs. (48) and (50) are equal to $1.0 \cdot 10^{-7}$ [m^2]. The maximal value of the cross sectional areas of the bars was assumed to be $1.0 \cdot 10^{-4}$ [m^2]. The maximal volume V in Eqs. (48), (50) is always equal to the initial volume of the truss considered: $V = V_{\text{init}}$ (with one exception in the example from Fig. 12 where the maximal volume $V = 4V_{\text{init}}$). Young modulus $E = 2.0 \cdot 10^8$ [kN/m^2].

5.1. Plane cantilever trusses

In the next examples optimal solutions are presented for only linear analysis of trusses, because the visible differences in layouts are rather small for the cases of loads that are below the critical values of bifurcation and limits points, as was mentioned above.

The first example is the cantilever truss (the layout from Fig. 1b, $N_r = 3$, $N_c = 6$, $L_x = 5.0$ [m], $L_y = 2.0$ [m]). The nodes along the left side of the truss are fixed and the single vertical force = 100.0 [kN] is applied at the middle of the right side of the truss cf. Fig. 2. Initial values of the compliance for the linear and non-linear cases are equal to 275.7 and 244.9 [kNm] respectively. Best compliances found by the method of moving asymptotes (MMA) for the linear and non-linear cases are equal to 111.0 and 114.8 [kNm] respectively. The convergence of the algorithm and the optimal layouts of the trusses in both cases are shown in Figs. 3 and 4 respectively. The greater the force

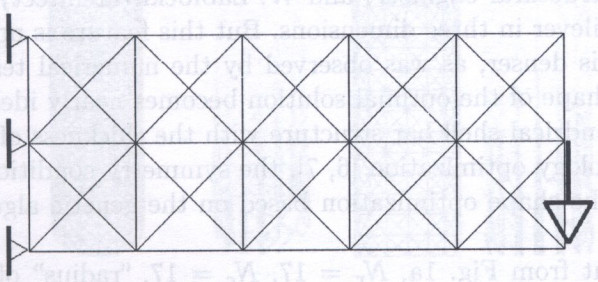

Fig. 2. Initial layout of the ground structure for transmitting a vertical force to a vertical line of supports

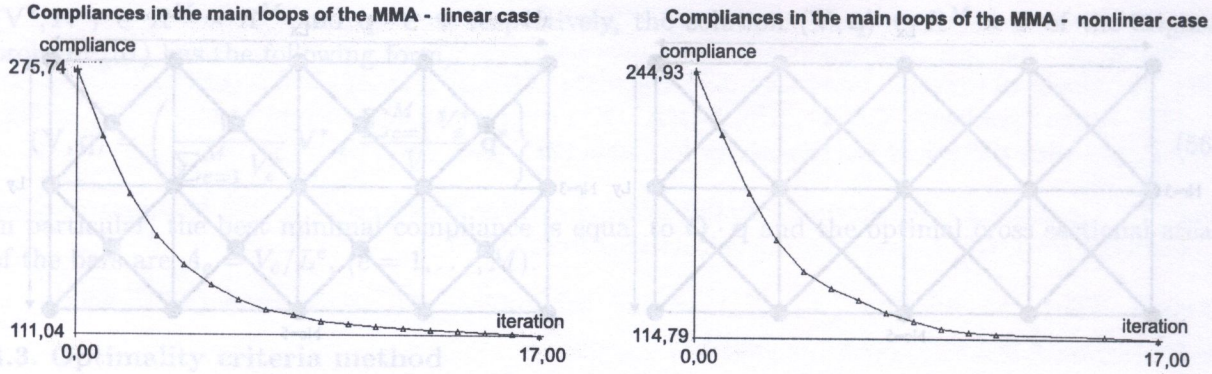

Fig. 3. Convergence of the MMA in the linear and non-linear case

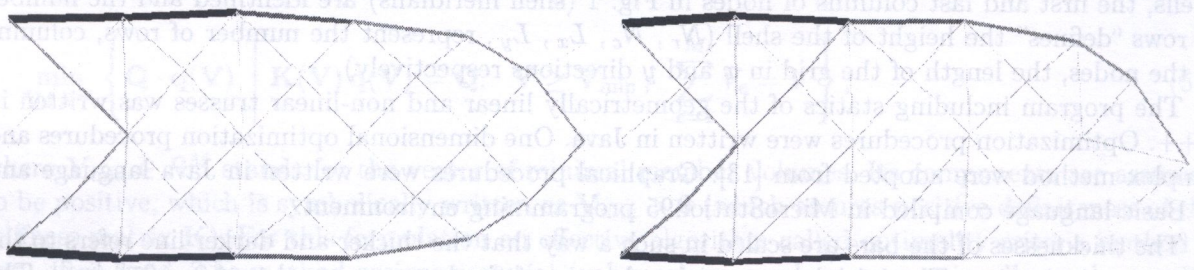

Fig. 4. Geometry and topology optimization (MMA). Optimal layouts in the linear and non-linear case

applied, the difference in the optimal layout in both cases turned out to be more distinct as the numerical tests have shown. However, the load was not taken too big, otherwise the more subtle and advanced static analysis should have been applied, see [4, 14]. The convergence of the MMA was generally good especially in the cases when the number of bars was not too big; the layouts obtained are satisfactory in comparison with the well known exact shapes of the Michell–Hemp cantilever [9–12]. The default rule for updating the "moving asymptotes" L_j, U_j given in [16] were successfully applied.

5.2. Cylindrical cantilever grid shells

The second example is the cylindrical cantilever grid shell cf. Fig. 5 (the layout from Fig. 1a, $N_r = 7$, $N_c = 7$, "radius" of the cylinder = 1.0 [m]). The nodes at the bottom side of the truss are fixed. The horizontal unit forces = 1.0 [kN] along X axis (horizontal at top view) are assumed to be put at all nodes (very simplified model of the wind load). The initial compliance is equal to 8.3 and the best compliance found by MMA is equal to 2.1 [kNm]. The optimal layout reminds, to some extent, the tulip like shape of the high-rise, multi-storeyed building, taller than 200 m, recently proposed by professors W. Zalewski (structural engineer) and W. Zabłocki (architect) [17–19] as a counterpart of the Michell–Hemp cantilever in three dimensions. But this feature is not a rule in the case when the initial layout of bars is denser, as was observed by the numerical tests. If the number of the bars is greater, then the shape of the optimal solution becomes nearly identical to its initial shape, i.e. resembles an ideal cylindrical shell bar structure with the thickness of the bars identical to the solution found by the topology optimization [6, 7]; the symmetry conditions on the position of the nodes are not imposed. The shape optimization based on the genetic algorithm also confirms this trend [7].

In Figs. 6–9 (the layout from Fig. 1a, $N_r = 17$, $N_c = 17$, "radius" of the cylinder = 1.0 [m]) the various optimal solutions of the similar cylindrical cantilever shell with denser initial grid layout are presented. The horizontal unit forces = 1.0 [kN] along Y axis (vertical at top view)

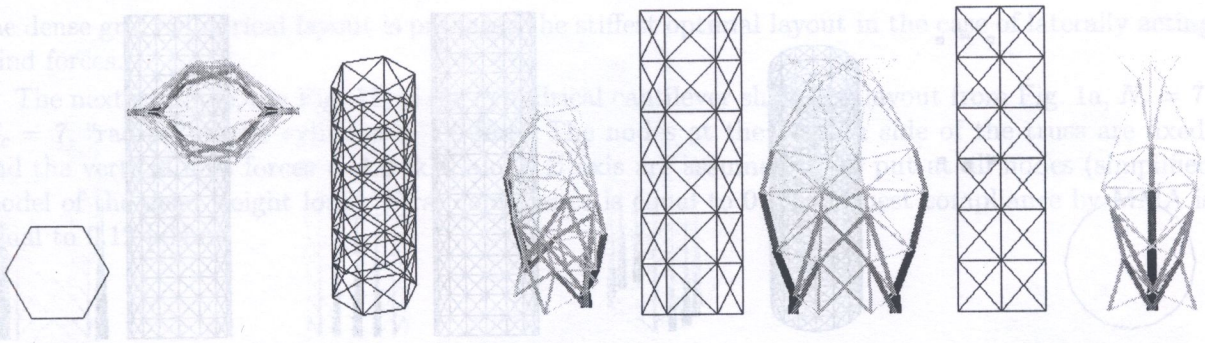

Fig. 5. Geometry and topology optimization (MMA). Initial and optimal layout: top view, right isometric view, front view and right view

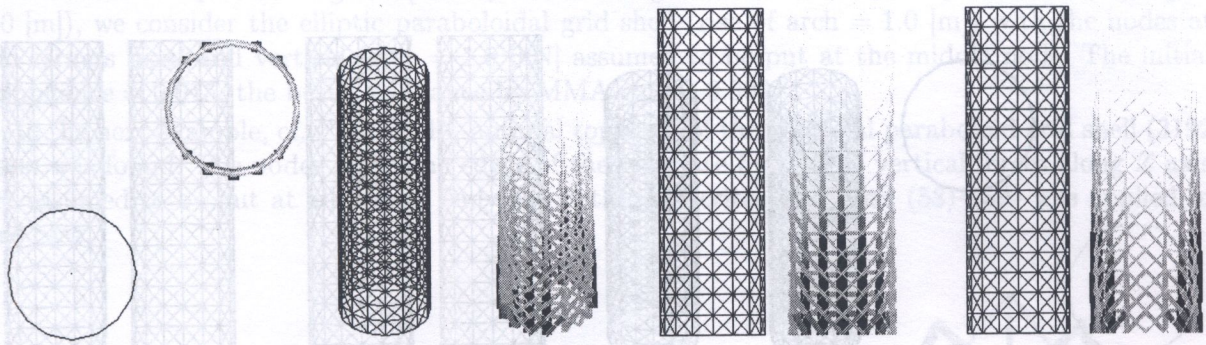

Fig. 6. Geometry and topology optimization (MMA). Initial and optimal layout: top view, right isometric view, front view and right view

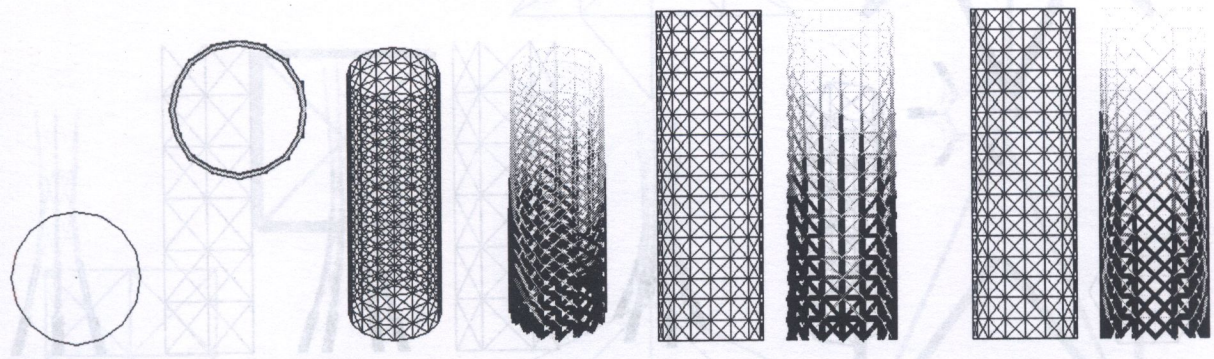

Fig. 7. Topology optimization (MMA). Initial and optimal layout: top view, right isometric view, front view and right view

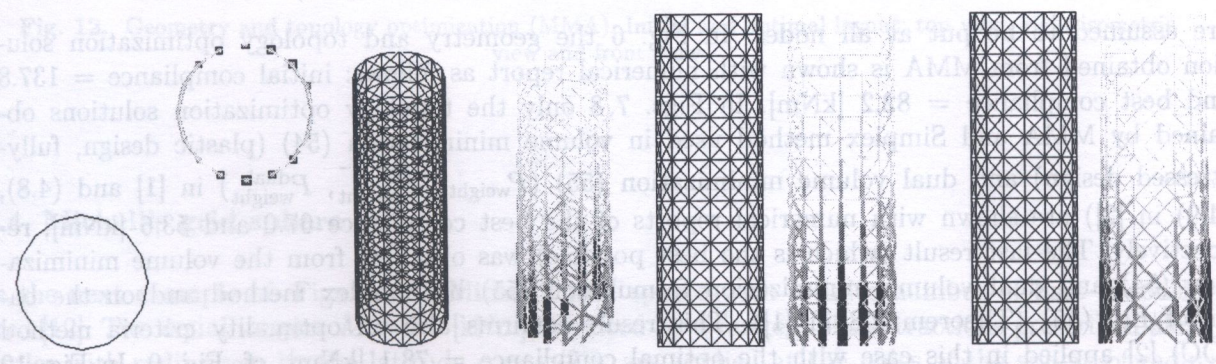

Fig. 8. Topology optimization (Simplex method). Initial and optimal layout: top view, right isometric view, front view and right view

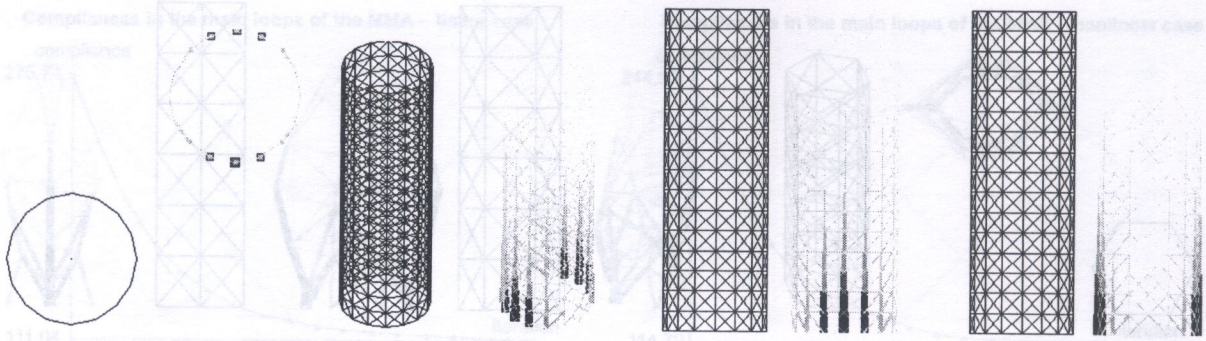

Fig. 9. Topology optimization (OC). Initial and optimal layout: top view, right isometric view, front view and right view

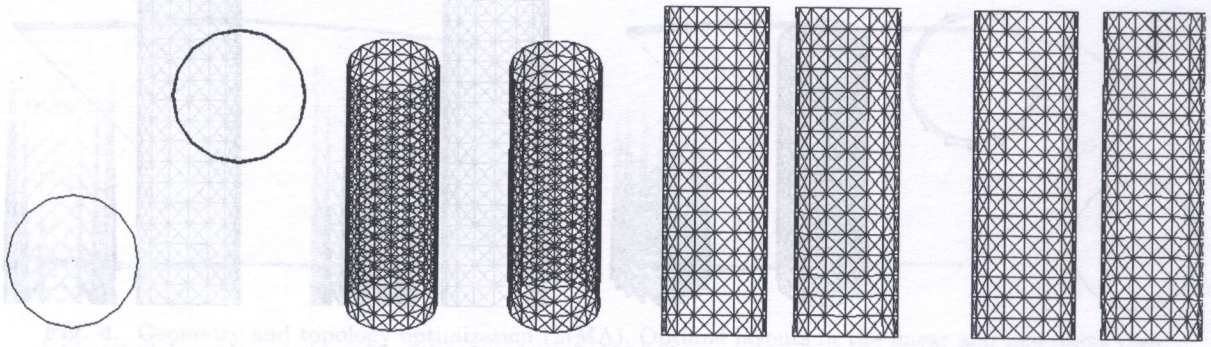

Fig. 10. Geometry optimization (MMA). Initial and optimal layout: top view, right isometric view, front view and right view

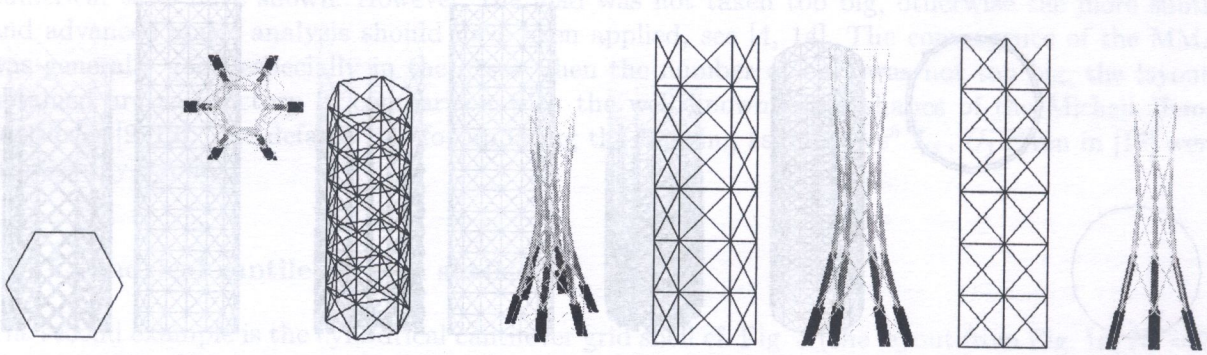

Fig. 11. Geometry and topology optimization (MMA). Initial and optimal layout: top view, right isometric view, front view and right view

are assumed to be put at all nodes. In Fig. 6 the geometry and topology optimization solution obtained from MMA is shown with numerical report as follows: initial compliance = 137.8 and best compliance = 82.2 [kNm]. In Figs. 7,8 only the topology optimization solutions obtained by MMA and Simplex method used in volume minimization (54) (plastic design, fully-stressed design) and dual volume minimization (55) (P_{weight}, $P^{q^+,q^-}_{\text{weight}}$, $P^{\text{dual}}_{\text{weight}}$) in [1] and (4.8), (4.9) in [2]) are shown with numerical reports of the best compliance 67.0 and 53.6 [kNm], respectively. The last result (which is the best possible) was obtained from the volume minimization (54) and dual volume minimization formulation (55) by Simplex method and on the basis of Eq. (56) (Theorem 2.8 in [1]). This result confirms also an optimality criteria method (OC) [2] applied in this case with the optimal compliance = 78.1 [kNm], cf. Fig. 9. In Fig. 10 only the geometry optimization solution is shown, obtained by MMA with the optimal value of compliance = 135.1 [kNm] which is only a little bit better then the initial compliance = 137.8. Thus

the dense grid cylindrical layout is probably the stiffest optimal layout in the case of laterally acting wind forces.

The next example, see Fig. 11, is the cylindrical cantilever shell (the layout from Fig. 1a, $N_r = 7$, $N_c = 7$, "radius" of the cylinder = 1.0 [m]). The nodes at the bottom side of the truss are fixed, and the vertical unit forces = 1.0 [kN] along Z axis are assumed to be put at all nodes (simplified model of the dead weight load). First compliance is equal to 0.47 and best compliance by MMA is equal to 0.12 [kNm].

5.3. Elliptic paraboloidal grid shells

In the next example, see Fig. 12 (the layout from Fig. 1a, $N_r = 3$, $N_c = 3$, $L_x = 2.0$ [m], $L_y = 2.0$ [m]), we consider the elliptic paraboloidal grid shell (rise of arch = 1.0 [m]) with the nodes at the corners fixed and vertical force = 1.0 [kN] assumed to be put at the middle node. The initial compliance = 0.015, the best compliance by MMA equals 0.002.

In the next example, cf. Figs. 13, 14, optimal topology of the elliptical paraboloid grid shell (3192 bars) was found. The nodes along the edges of the truss are fixed. The vertical forces along Z axis are assumed to be put at all nodes. Only the optimality criteria method (58)–(59) was applied in this case.

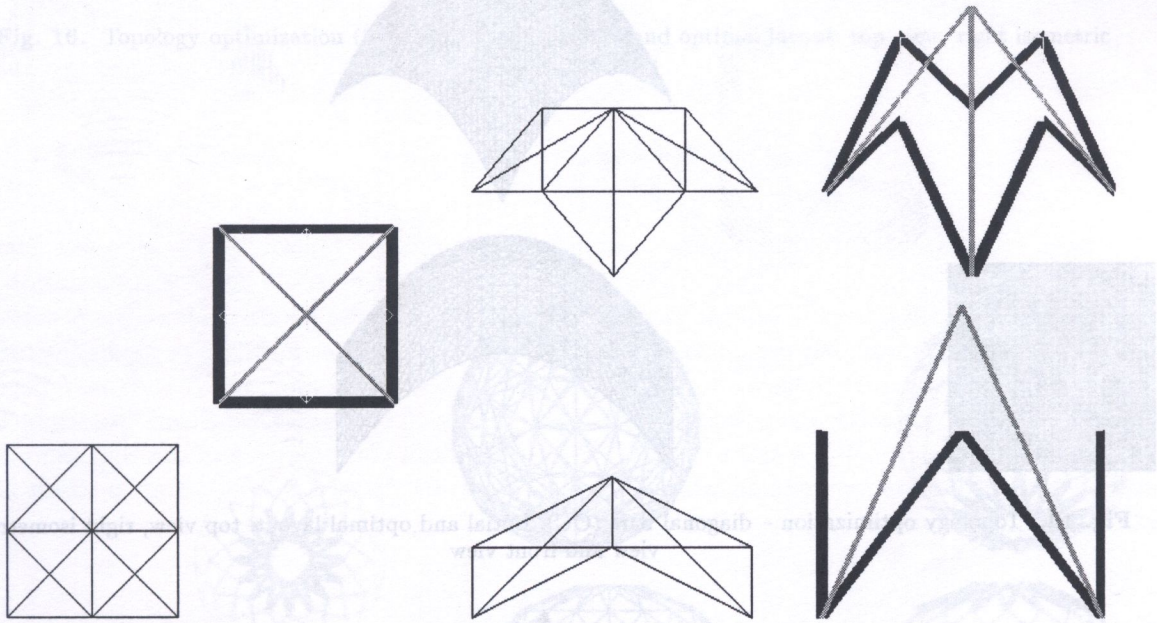

Fig. 12. Geometry and topology optimization (MMA). Initial and optimal layout: top view, right isometric view and front view

5.4. Michell's grid sphere

In the next example cf. Figs. 15–18 Michell's grid sphere with a finite number of bars is considered [12]. Two equal torques $M = 1.0$ [kNm], replaced by a tangent shear tractions prescribed along circles with radii given by the latitude $\alpha = \pi/2.3$, are applied at the poles of the sphere of radius $r = 1.0$ [m]. Let $\sigma_T = \sigma_C = \sqrt{E}$ denote the stresses allowed for tension and compression with $E = 208$ [GPa].

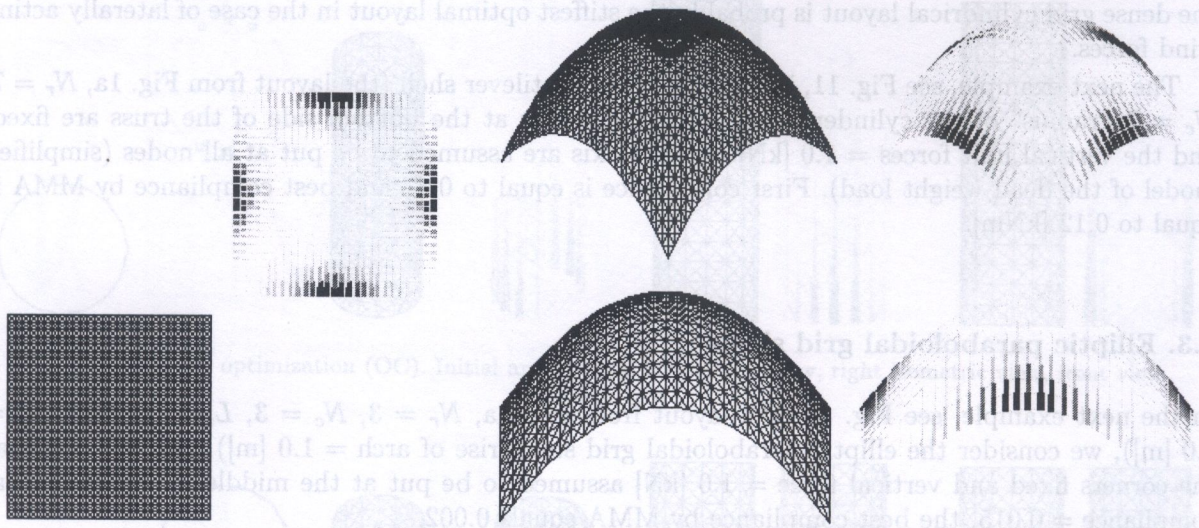

Fig. 13. Topology optimization – horizontal and vertical bars (OC). Initial and optimal layout: top view, right isometric view and front view

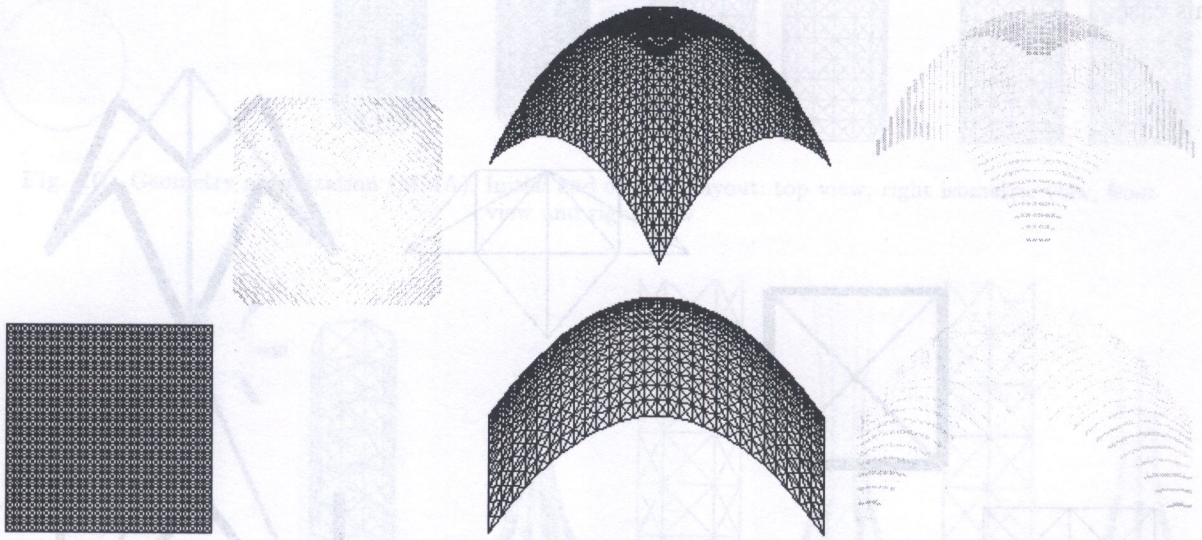

Fig. 14. Topology optimization – diagonal bars (OC). Initial and optimal layout: top view, right isometric view and front view

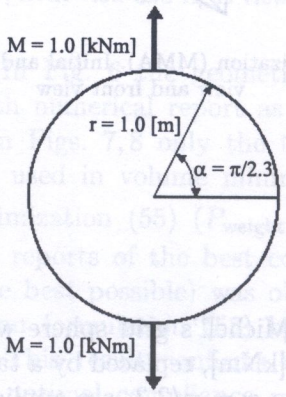

Fig. 15. Side view of the Michell sphere. Data values for the topology optimization by MMA, OC and Simplex method

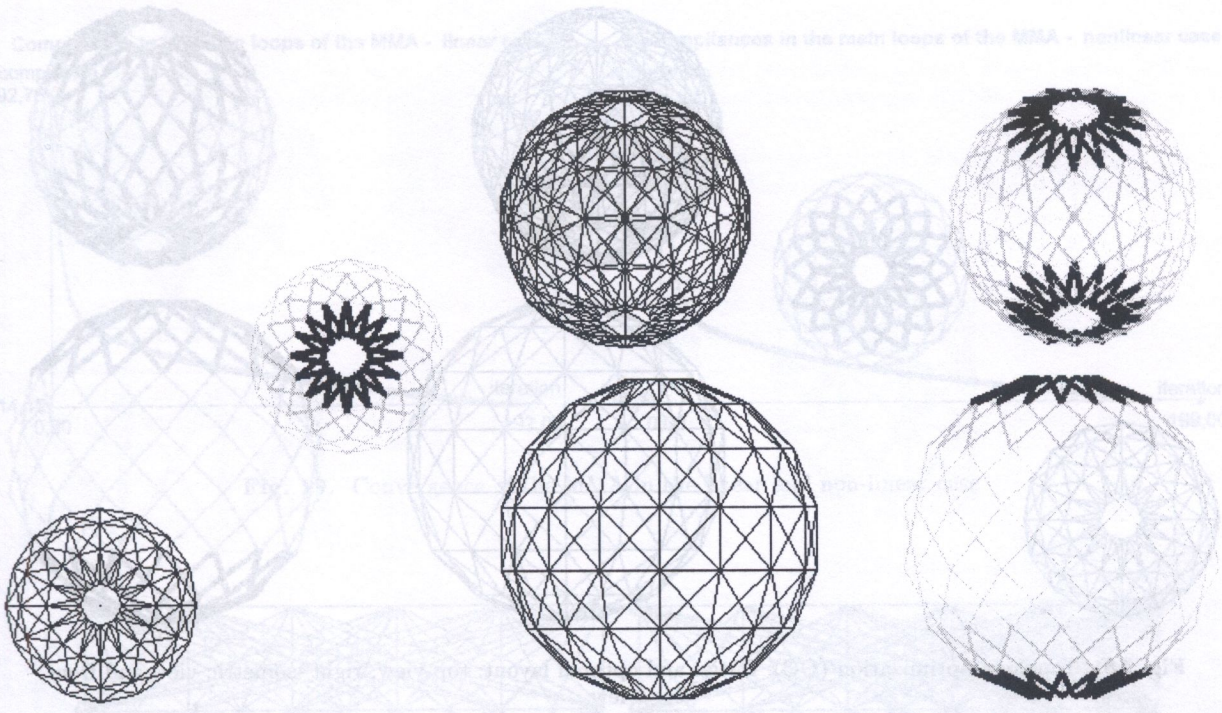

Fig. 16. Topology optimization (Simplex method). Initial and optimal layout: top view, right isometric view and front view

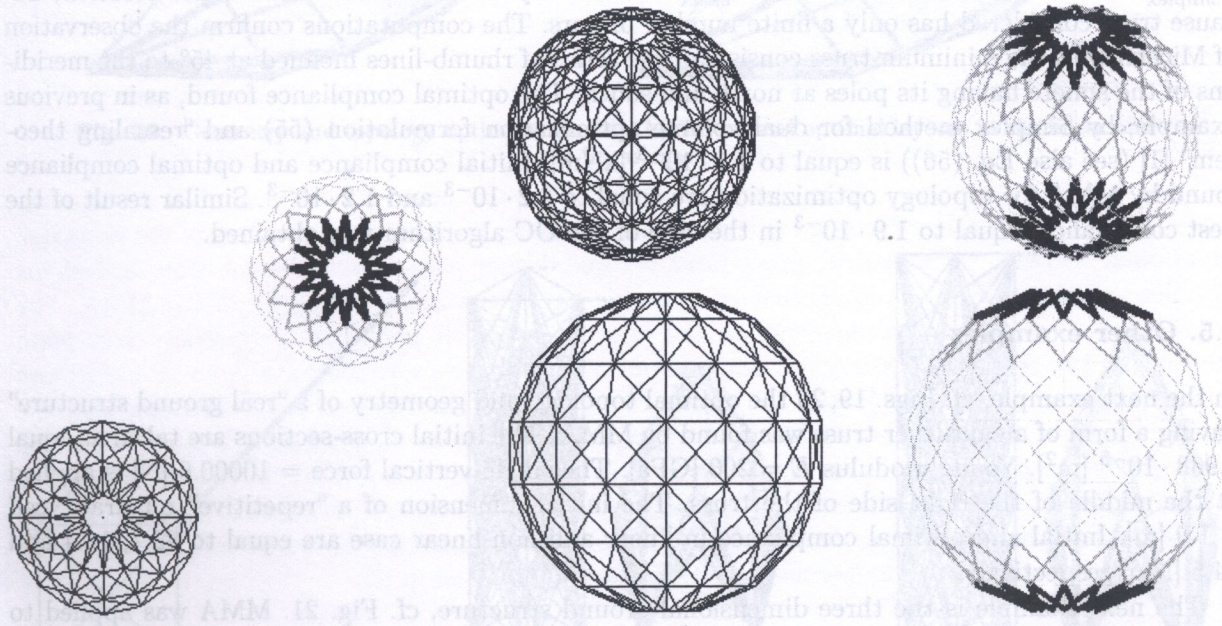

Fig. 17. Topology optimization (MMA). Initial and optimal layout: top view, right isometric view and front view

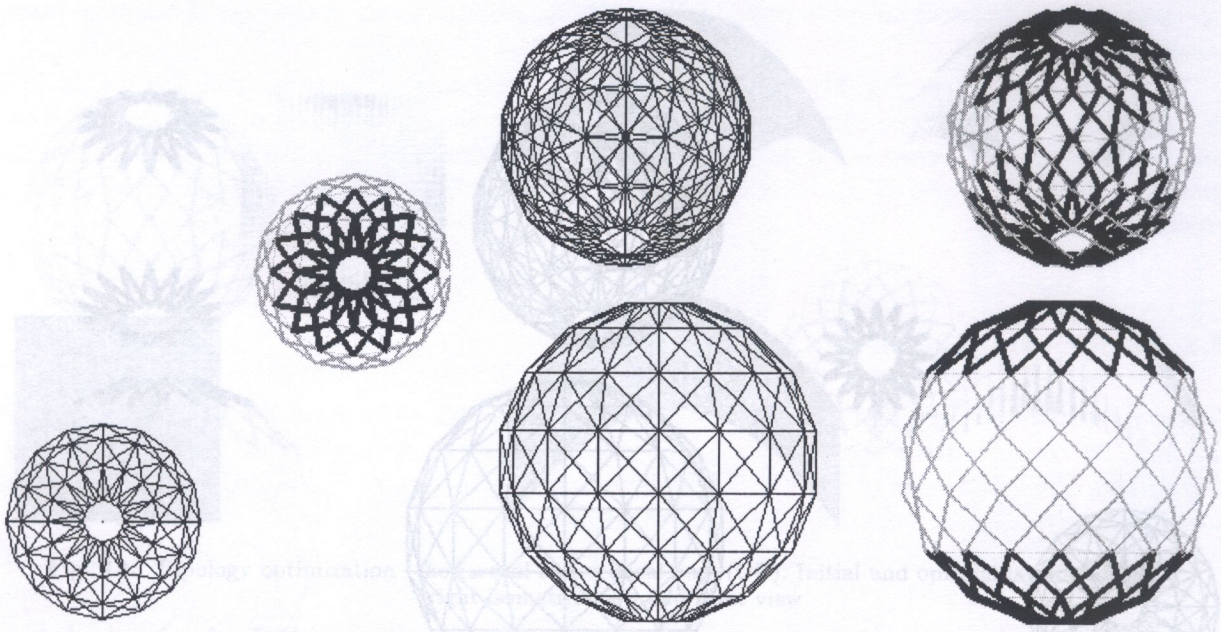

Fig. 18. Topology optimization (OC). Initial and optimal layout: top view, right isometric view and front view

The Michell formula [12] – exact solution – for the minimum volume of the pseudo-continuum sphere reads

$$V_{\text{exact}}^{\text{opt}} = \frac{2 \cdot M}{r} \cdot \left(\frac{1}{\sigma_T} + \frac{1}{\sigma_C} \right) \cdot \ln \left[\tan \left(\frac{\pi}{4} + \frac{\alpha}{2} \right) \right] \approx 6.4 \cdot 10^{-4}. \tag{60}$$

Optimal truss volume in the volume minimization problem found by the Simplex method $V_{\text{simplex}}^{\text{opt}} \approx 9.0 \cdot 10^{-4} > 6.4 \cdot 10^{-4} \approx V_{\text{exact}}^{\text{opt}}$ is obviously a worse result than exact solution, because truss considered has only a finite number of bars. The computations confirm the observation of Michell that the minimum truss consists of the series of rhumb-lines inclined at 45° to the meridians of the sphere having its poles at north and south. The optimal compliance found, as in previous example, by Simplex method for dual volume optimization formulation (55) and "rescaling theorem" [1] (see also Eq. (56)) is equal to $1.1 \cdot 10^{-3}$ [kNm]. Initial compliance and optimal compliance found by MMA for topology optimization are equal to $3.2 \cdot 10^{-3}$ and $1.2 \cdot 10^{-3}$. Similar result of the best compliance, equal to $1.9 \cdot 10^{-3}$ in the case of the OC algorithm was obtained.

5.5. Other examples

In the next example, cf. Figs. 19, 20 the optimal topology and geometry of a "real ground structure" having a form of a cantilever truss was found by MMA. The initial cross-sections are taken as equal $1.963 \cdot 10^{-5}$ [m^2]. Young modulus $E = 200$ [GPa]. The single vertical force = 10000.0 [N] is applied at the middle of the right side of the truss. The initial dimension of a "repetitive" quadratic cell is 1.0 [m]. Initial and optimal compliance in linear and non-linear case are equal to 92.7, 14.4 and 14.5 [Nm] respectively.

The next example is the three dimensional ground structure, cf. Fig. 21. MMA was applied to find the optimal topology and shape. The forces in the directions: horizontal and parallel to the diagonal of the projection of the structure are applied only at the top nodes of the cantilever.

The last example is based on the three dimensional ground structure, cf. Fig. 22. The MMA method is applied to find the optimal topology and shape. Vertical forces were applied only at the top nodes of the of the parallelepiped.

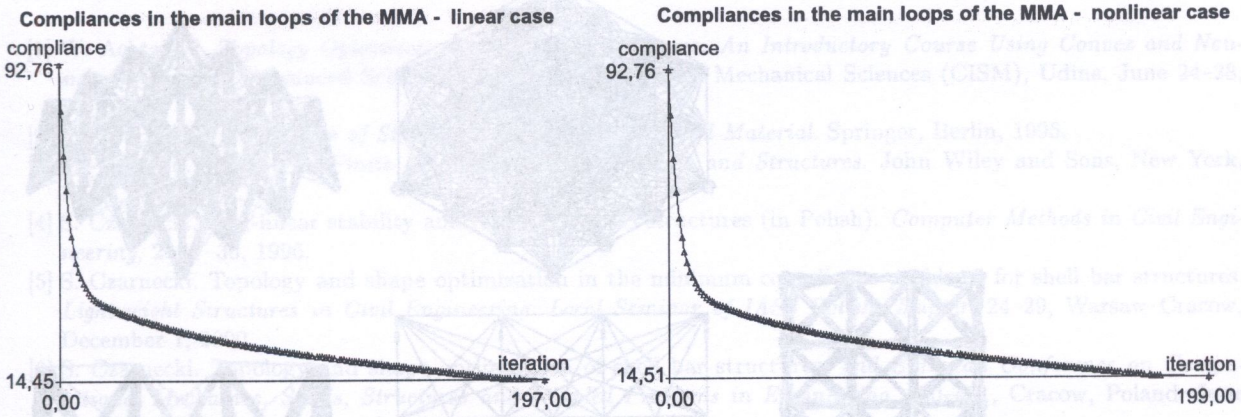

Fig. 19. Convergence of the MMA in the linear and non-linear case

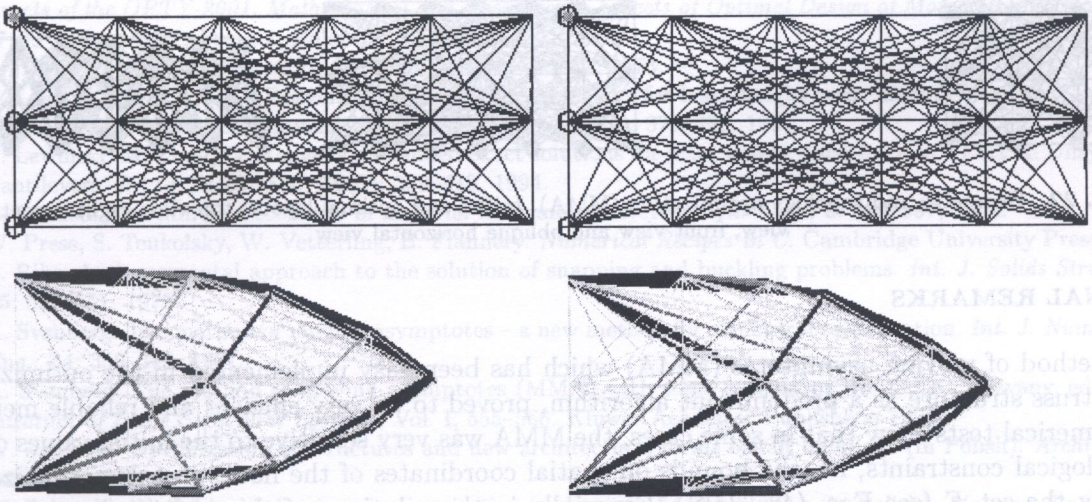

Fig. 20. Geometry and topology optimization (MMA). Initial and optimal layouts in the linear and non-linear case

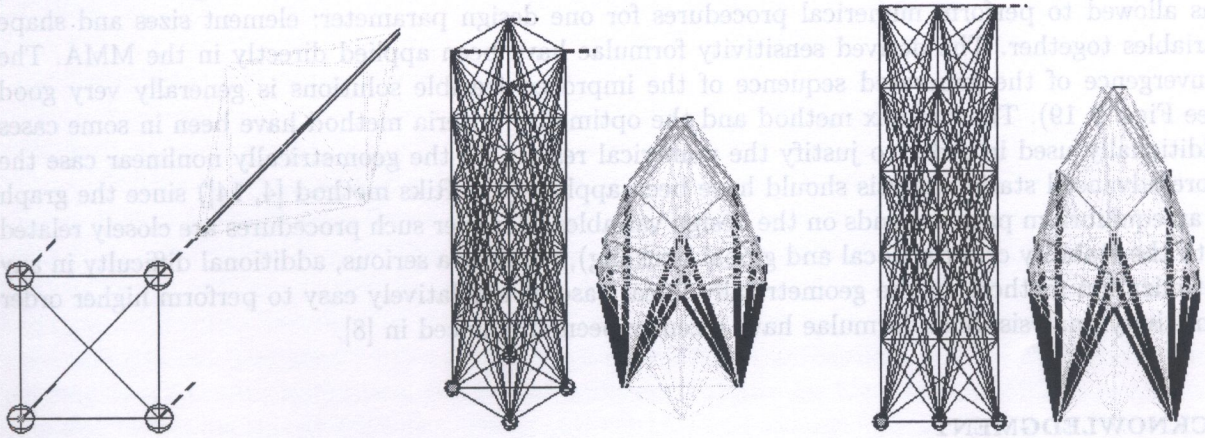

Fig. 21. Geometry and topology optimization (MMA). Initial and optimal layout: top view, right isometric view and oblique horizontal view

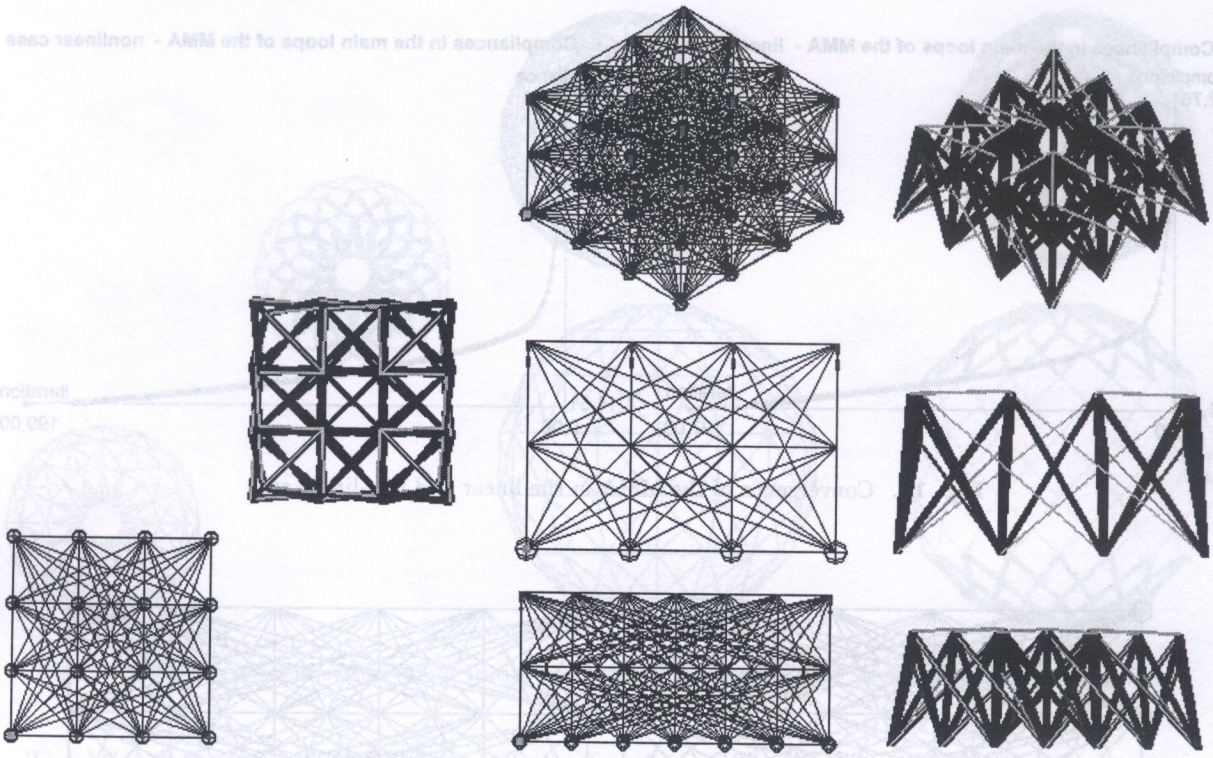

Fig. 22. Geometry and topology optimization (MMA). Initial and optimal layout: top view, right isometric view, front view and oblique horizontal view

6. Final remarks

The method of moving asymptotes (MMA) which has been easy implemented in the optimization of the truss structure as a predominant algorithm, proved to be very efficient and reliable method, but numerical tests show that in some cases, the MMA was very sensitive to the initial values of the technological constraints, i.e. the bounds on spatial coordinates of the nodes in truss optimization defining the set F (see Eqs. (48), (50)). Especially in the solutions of the rotational symmetrical shell bar structures with greater number of bars, the symmetry of the optimal layout was sometimes difficult to obtain when the bounds were too wide. The MMA is able to handle not only cross sectional areas of the bars as design parameters, but also, the geometrical parameters – the nodal points location. The main advantage of this method – the insensibility to the scaling of the variables, has allowed to perform numerical procedures for one design parameter: element sizes and shape variables together. The derived sensitivity formulae have been applied directly in the MMA. The convergence of the generated sequence of the improved feasible solutions is generally very good (see Figs. 3, 19). The simplex method and the optimality criteria method have been in some cases additionally used in order to justify the numerical results. In the geometrically nonlinear case the more advanced static analysis should have been applied (e.g. Riks method [4, 14]) since the graph of an equilibrium path depends on the design variables. However such procedures are closely related with the stability criteria (local and global buckling), which is a serious, additional difficulty in any optimization method. In the geometrically linear case, it is relatively easy to perform higher order sensitivity analysis. Such formulae have recently been announced in [8].

Acknowledgment

This work was supported by the Polish Committee for Scientific Research (KBN) through the Grant No 7 T07A 04318

REFERENCES

[1] W. Achtziger. *Topology Optimization of Discrete Structures: An Introductory Course Using Convex and Non-smooth Analysis.* Advanced School, International Centre for Mechanical Sciences (CISM), Udine, June 24–28, 1996.

[2] M. Bendsøe. *Optimization of Structural Topology, Shape, and Material.* Springer, Berlin, 1995.

[3] M. Crisfield. *Non-linear Finite Element Analysis of Solids and Structures.* John Wiley and Sons, New York, 1991.

[4] S. Czarnecki. Non-linear stability analysis of the truss structures (in Polish). *Computer Methods in Civil Engineering*, **2**: 17–30, 1996.

[5] S. Czarnecki. Topology and shape optimization in the minimum compliance problems for shell bar structures. *Lightweight Structures in Civil Engineering. Local Seminar of IASS Polish Chapter*, 24–29, Warsaw–Cracow, December 1, 2000.

[6] S. Czarnecki. Topology and shape optimization of shell bar structures. *2nd European Conference on Computational Mechanics. Solids, Structures and Coupled Problems in Engineering.* 430–431, Cracow, Poland, June 26–29, 2001.

[7] S. Czarnecki. Numerical comparative analysis of the selected algorithms in topology and shape optimization of the truss structures (in Polish). Research work No. 503/1111, Institute of Structural Mechanics, Warsaw University of Technology, June 2001.

[8] S. Czarnecki. Compliance optimization in shape and topology designing of the truss structures. In: *Book of Abstracts of the OPTY-2001, Mathematical and Engineering Aspects of Optimal Design of Materials and Structures*, 27–29 August 2001, Poznań, Poland.

[9] W. Hemp. *Optimum Structures.* Clarendon Press, Oxford, 1973.

[10] T. Lewiński, M. Zhou, G. Rozvany. Extended exact solutions for least weight truss layouts – Part I: Cantilever with a horizontal axis of symmetry. *Int. J. Mech. Sci.*, **36**(5): 375–398, 1994.

[11] T. Lewiński, M. Zhou, G. Rozvany. Extended exact solutions for least weight truss layouts – Part II: Unsymetric Cantilevers. *Int. J. Mech. Sci.*, **36**(5): 399–419, 1994.

[12] A. Michell. The limits of economy of material in frame structures. *Phil. Mag.*, **8**: 589–597, 1904.

[13] W. Press, S. Teukolsky, W. Vetterling, B. Flannery. *Numerical Recipes in C.* Cambridge University Press, 1992.

[14] E. Riks. An incremental approach to the solution of snapping and buckling problems. *Int. J. Solids Structures*, **15**: 529–551, 1979.

[15] K. Svanberg. The method of moving asymptotes – a new method for structural optimization. *Int. J. Num. Meth. Eng.*, **24**: 359–373, 1987.

[16] K. Svanberg. The method of moving asymptotes (MMA) with some extensions. In: G.I.N. Rozvany, ed., *Optimization of Large Structural Systems*, Vol. I, 555–566. Kluwer Academic Publishers, 1993.

[17] W. Zabłocki. Optimization of structures and new architectural forms of tall buildings (in Polish). *Architektura*, **74**: 96–98, 2000.

[18] W. Zalewski, W. Zabłocki. Engineering inspiration in shaping of tall buildings (in Polish). *Magazyn Budowlany*, **8**: 50–54, 1999.

[19] W. Zalewski. The strength and the lightness – the muses of a structural engineer (in Polish). *Architektura*, **74**: 94–95, 2000.